J Electr Eng Technol Vol. 8, No. 4: 899-910, 2013
http://dx.doi.org/10.5370/JEET.2013.8.4.899

ISSN(Print) 1975-0102
ISSN(Online) 2093-7423

Lateral Stability Control of Electric Vehicle Based On Disturbance Accommodating Kalman Filter using the Integration of Single Antenna GPS Receiver and Yaw Rate Sensor

Binh-Minh Nguyen†, Yafei Wang, Hiroshi Fujimoto* and Yoichi Hori***

Abstract – This paper presents a novel lateral stability control system for electric vehicle based on sideslip angle estimation through Kalman filter using the integration of a single antenna GPS receiver and yaw rate sensor. Using multi-rate measurements including yaw rate and course angle, time-varying parameters disappear from the measurement equation of the proposed Kalman filter. Accurate sideslip angle estimation is achieved by treating the combination of model uncertainties and external disturbances as extended states. Active front steering and direct yaw moment are integrated to manipulate sideslip angle and yaw rate of the vehicle. Instead of decoupling control design method, a new control scheme, "two-input two-output controller", is proposed. The extended states are utilized for disturbance rejection that improves the robustness of lateral stability control system. The effectiveness of the proposed methods is verified by computer simulations and experiments.

Keywords: Electric vehicle, GPS, Lateral stability control, Kalman filter

1. Introduction

The remarkable advantages of in-wheel motors have greatly improved the motion control of electric vehicles (EVs) [1]. Firstly, torque response of EV is very quick in comparison with that of internal combustion engine vehicle. Secondly, yaw moment generated by in-wheel motors can be used as a control input to the vehicle. Finally, road condition is identified based on accurate motor torque measurements. Lateral stability control is considered as one of the critical issues in EV motion control. Yaw rate control alone is inadequate for keeping the vehicle moving on low friction road at high speed. Both yaw rate and sideslip angle must be controlled to follow the reference values calculated from driver's inputs [2]. While yaw rate can be measured using low cost gyroscopes, sideslip angle sensors are very expensive for installation into commercial vehicles. In order to keep the cost down while improving the safety of EVs, the sideslip angle estimator plays an important role in lateral stability control system.

Sideslip angle estimation methods can be categorized into three groups: kinematic model-based estimation [3-4], nonlinear dynamic model-based estimation [5-6], and linear dynamic model-based estimation [7-8]. Kinematic model based estimation does not rely on the tire force characteristics of the vehicle. However, it uses acceleration measurements which are always corrupted with strong noises. Moreover, roll angle and road inclination introduces offset to lateral acceleration sensor signals due to gravity. Therefore, kinematic model-based estimator cannot satisfy the requirement of stability and robustness in long-term operation. Although nonlinear observer has been developed theoretically, the nonlinear model is complicated to implement in real time. On the other hand, linear estimation using constant vehicle parameters is not robust enough under the variation of road friction coefficient. In [9], adaptive estimation of sideslip angle is proposed. However, the integration of an observer with an online cornering stiffness identifier increases the computational burden of the control system. The accuracy of sideslip angle estimation relies on the accuracy of cornering stiffness identification and vice versa. If the road condition suddenly change (for instance, from high friction to low friction), the sideslip angle estimation cannot be accurate until the estimated cornering stiffness converge to the true values. Therefore, it is essential to study the estimation methods that are robust to the big change of road condition.

In recent years, robust estimation using nonconventional sensors has been studied. Visual information can provide heading angle and lateral distance of a vehicle for sideslip angle estimation [10]. However, visual signal may be unavailable when road markers are covered with leaves, snow, water, or dirt. In [11], based on the difference between the left and right tire lateral force measurements, sideslip angle identification without cornering stiffness is proposed. However, the high cost and the influence of strong noises are big hurdles in using tire force sensors in vehicle motion control.

Since the last decade, global positioning system (GPS)

† Corresponding Author: Dept. of Advanced Energy, the University of Tokyo, Japan. (minh@hori.k.u-tokyo.ac.jp)
* Dept. of Advanced Energy, the University of Tokyo, Japan. ({fujimoto, hori}@k.u-tokyo.ac. jp)
** Dept. of Electrical Engineering, the University of Tokyo, Japan. (wang@hori.k.u-tokyo.ac.jp)
Received: May 27, 2013; Accepted: June 7, 2013

has been a candidate for vehicle state estimation. The fusion of GPS receiver with on-board dynamic sensors can provide accurate state estimation in long-term operation. GPS can be used to measure not only vehicle positions, but also velocity and attitude. By using a double-antenna GPS receiver, sideslip angle can be calculated directly [12]. A single-antenna GPS receiver can be combined with a yaw rate sensor to estimate both sideslip angle and yaw angle using a Kalman filter [13]. In [14], the integration of single antenna GPS and a magnetometer introduces a new method for sideslip angle estimation. Due to the poor update rate of GPS receiver (1-10 Hz), the method proposed in [12] cannot satisfy the requirement of advanced motion control of EVs in which the control signals are generated every 1 millisecond. The fusion of GPS receiver and yaw rate sensor in [13] can provide high-rate sideslip angle estimation. However, the robustness of estimation under model uncertainties and external disturbances was not examined. In [14], the using of magnetometer increases the cost of this method. Moreover, the methods proposed in [12-14] have not been integrated with the controllers in real-time control system of vehicles.

In this paper, sideslip angle estimation based on a Kalman filter that takes single-antenna GPS receiver and yaw rate sensor is proposed. Following the idea of disturbance accommodating control [15], by treating the model uncertainties and external disturbances as extended states, high accuracy of estimation is achieved. An important advantage of the proposed estimator is that yaw angle (heading angle) can be estimated. The estimated yaw angle can be used for other purposes, such as vehicle attitude control or vehicle position estimation. Active front steering and direct yaw moment are selected as control inputs for manipulating both yaw rate and sideslip angle. Instead of decoupling control scheme, a new "two-input two-output controller" is proposed. Using this method, the decoupling term is unnecessary to be designed. Therefore, the robustness of the decoupling term under the variation of vehicle model is not a problem in this study. The robustness of the system is also improved based on disturbance estimation and rejection using Kalman filter.

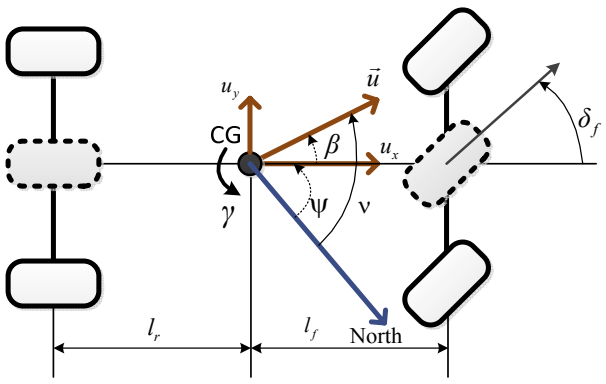

Fig. 1. Planar bicycle model of electric vehicle

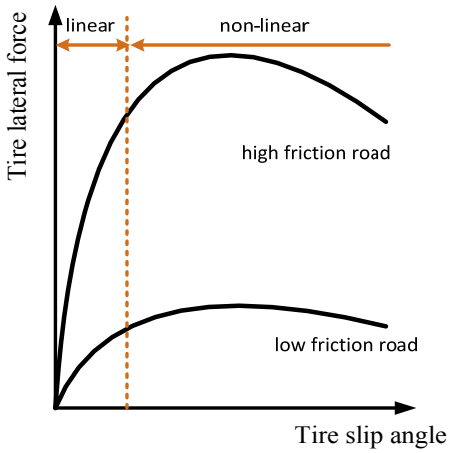

Fig. 2. Tire lateral force characteristics

Table 1. Nomenclatures

l_f, l_r	Distances from front and rear axle to CG
C_f, C_r	Front and rear cornering stiffness
I_z	Yaw moment of inertia
δ_f, N_z	Front steering angle, yaw moment
M	Vehicle mass
β, γ	Sideslip angle, yaw rate
ψ, ν	Yaw angle, course angle from GPS
u_x,u_y	Longitudinal and lateral velocity

2. Vehicle Modeling

The linear bicycle model shown in Fig. 1 is constructed under the following assumptions: 1) Tire slip angle is small so that the lateral component of tire force is within linear region as shown in Fig. 2. 2) Vehicle is symmetric about the fore-and-aft center line. 3) Load transfer, roll motion, and pitch motion are neglected.

During operation, external disturbances (lateral wind force, for instance) frequently interfere with the vehicle system. The influence of external disturbances can be generalized by lateral force disturbance F_d and yaw moment disturbance N_d. The lateral force equation and yaw moment equation can be expressed as follows:

$$Mu_x\left(\dot{\beta}+\gamma\right)=-2C_f\left(\beta+\frac{l_f\gamma}{u_x}-\delta_f\right)-2C_r\left(\beta-\frac{l_r\gamma}{u_x}\right)+F_d \tag{1}$$

$$I_z\dot{\gamma}=-2C_f\left(\beta+\frac{l_f\gamma}{u_x}-\delta_f\right)l_f+2C_r\left(\beta-\frac{l_r\gamma}{u_x}\right)l_r+N_z+N_d \tag{2}$$

Course angle of a moving vehicle is defined as the angle between vehicle's velocity vector and the geodetic North, as shown in Fig. 1. Course angle is represented as the sum

of yaw angle and sideslip angle as follows:

$$\nu = \psi + \beta \tag{3}$$

3. Experimental System

A micro in-wheel motored EV named "Super-capacitor COMS" developed by EV team of Hori-Fujimoto Lab is used in this study (Fig. 3). Two in-wheel motors are placed in the rear-left and rear-right wheels. Thus, torque command can be distributed independently to each wheel to generate a yaw moment. Active front steering system is used as another control actuator which enables the steer-by-wire mode. The vehicle is also equipped with a gyroscope and accelerometers to measure yaw rate, longitudinal acceleration, and lateral acceleration. In addition, a noncontact optical sensor, Correvit (produced by Corrsys-Datron), is used for accurate acquisition of vehicle sideslip angle, longitudinal velocity, and lateral velocity. In this paper, it is used for evaluating the performance of the proposed estimation algorithm. Although it is placed at the front of the EV, sideslip angle at the center of gravity can be derived based on the vehicle geometry with the use of yaw rate measurement. Estimation and control algorithms are implemented in a RT-Linux operating system computer which is used as a main controller. The fundamental control period of the system is 1 millisecond. The specifications of the experimental EV are summarized in Table 2.

GPS receiver CCA-600 provided by Japan Radio Co. Ltd. is used in this study. Table 3 shows the main features of CCA-600. It can provide not only vehicle positioning but also velocity and course angle. We design GPS software

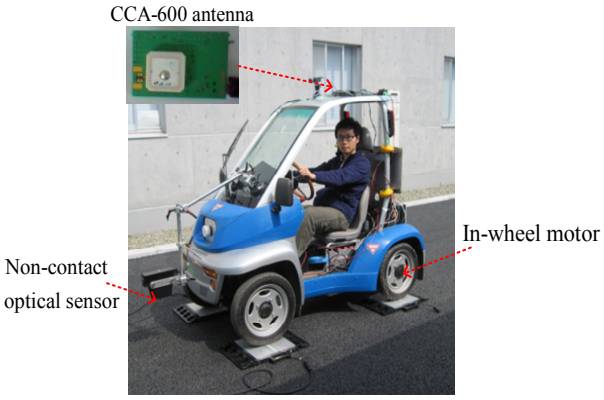

Fig. 3. Experimental electric vehicle and GPS receiver

with the following functions: 1) Decoding of the NMEA output messages from CCA-600 and displaying the navigation data. 2) Transferring of the motion measurement data to the main controller. 3) Recording the experimental data. The software is implemented in a laptop to receive the NMEA messages from serial port, and then to send the decoded data through LAN cable to EV's controller.

A view of the GPS software's interface is shown in Fig. 4. Using the software we can receive the GPS receiver's dilution of precision (DOP), the detailed information of satellites in view like carrier-to-noise ratio (CNR). Such kind of information is essential for evaluating the accuracy of GPS measurement in real time. Fig. 4 also shows the vehicle positions on Google Earth, vehicle velocity and course angle obtained from an experiment. The software can also transfer the position on longitude-latitude coordinates to the planar North-East coordinates and calculate the driving distance of the vehicle.

Fig. 4. GPS software interface and experimental data

Table 2. Specifications of experimental EV

Total mass	400 kg
Wheel base	1.2 m
Track-width of rear wheel	0.82 m
Height of CG	0.4 m
Wheel radius	0.26 m
Wheel spin inertia	1.26 kgm^2
Yaw moment of inertia	136 kgm^2
Energy store (super-capacitor)	210V, 29F, 173 Wh
Main controller	PC104, Linux OS
In-wheel motor type	PMSM
Max. motor power	2 kW
Max. motor torque	100 Nm
Max. vehicle velocity	50 km/h

Table 3. Features of GPS receiver CCA-600

Receiving method	L1(1575.42 MHz)GPS (C/A)
Augmentation method	Satellite based (SBAS)
Positioning accuracy	2.5 m CEP
Course angle accuracy	0.14 degree RMS
Velocity accuracy	0.05 m/s RMS
Data format	NMEA-0183
Current consumption	36 mA
Update rate	5 Hz

4. Sideslip Angle Estimation Design

4.1 Disturbance accommodating dynamic model

Basically, the estimation model is designed using nominal values of cornering stiffness: C_{fn} and C_{rn}. Due to the change of road condition, the nominal cornering stiffness differs from the true values. The variation of tire cornering stiffness can be expressed by the following equations:

$$\begin{cases} C_f = C_{fn} + \Delta C_f \\ C_r = C_{rn} + \Delta C_r \end{cases} \tag{4}$$

From (1)-(4), a state space model of vehicle dynamics can be derived as (5)-(10) in which the unknown input disturbance d_1 and d_2 represent the combined influence of external disturbances and cornering stiffness variation. The input vector u includes the front steering angle and yaw moment generated by in-wheel motors and w is the process noise vector. In (7), a_{n11}, .., a_{n22}, b_{n11}, …, b_{n22} are calculated using the nominal vehicle parameters (detailed formulation are presented in the Appendix).

$$\dot{x} = A_n x + B_n u + D_n \varsigma + w \tag{5}$$

$$x = \begin{bmatrix} \beta & \gamma & \psi \end{bmatrix}^T, u = \begin{bmatrix} \delta_f & N_z \end{bmatrix}^T, \varsigma = \begin{bmatrix} d_1 & d_2 \end{bmatrix}^T \tag{6}$$

$$A_n = \begin{bmatrix} a_{n11} & a_{n12} & 0 \\ a_{n21} & a_{n22} & 0 \\ 0 & 1 & 0 \end{bmatrix}, B_n = \begin{bmatrix} b_{n11} & b_{n12} \\ b_{n21} & b_{n22} \\ 0 & 0 \end{bmatrix}, D_n = \begin{bmatrix} 1 & 0 \\ 0 & 1 \\ 0 & 0 \end{bmatrix} \tag{7}$$

$$d_1 = \frac{-2\left(\Delta C_f + \Delta C_r\right)}{Mu_x}\beta + \frac{-2\left(\Delta C_f l_f - \Delta C_r l_r\right)}{Mu_x^2}\gamma + \frac{2\Delta C_f}{Mu_x}\delta_f + \frac{1}{Mu_x}F_d \tag{8}$$

$$d_2 = \frac{-2\left(\Delta C_f l_f - \Delta C_r l_r\right)}{I_z}\beta + \frac{-2\left(\Delta C_f l_f^2 + \Delta C_r l_r^2\right)}{I_z u_x}\gamma + \frac{2\Delta C_f l_f}{I_z}\delta_f + \frac{1}{I_z}N_d \tag{9}$$

The continuous time model (5) is transformed to the discrete time model (10) by using the transformation (11) in which T_c is the fundamental sampling time (1 millisecond in this paper).

$$x_{k+1} = A_{nd} x_k + B_{nd} u_k + D_{nd} \varsigma_k + w_k \tag{10}$$

$$A_{nd} = e^{A_n T_c},\ B_{nd} = \int_0^{T_c} e^{A_n \tau} d\tau B_n,\ D_{nd} = \int_0^{T_c} e^{A_n \tau} d\tau D_n \tag{11}$$

In [15], disturbance accommodating control was firstly introduced to control theory. The original idea is that the external disturbances can be augmented to be extended states. In this paper, this idea is applied in Kalman filter for sideslip angle estimation by assuming the unknown input terms can be considered as stochastic processes with zero-mean white noise sequence:

$$\varsigma_{k+1} = \varsigma_k + w_{dis,k} \tag{12}$$

Based on the assumption (12), a new state space model is constructed as follows:

$$X_{k+1} = \tilde{A}_{nd} X_k + \tilde{B}_{nd} U_k + W_k \tag{13}$$

$$X_k = \begin{bmatrix} x_k \\ \varsigma_k \end{bmatrix},\ U_k = u_k,\ W_k = \begin{bmatrix} w_k \\ w_{dis,k} \end{bmatrix} \tag{14}$$

$$\tilde{A}_{nd} = \begin{bmatrix} A_{nd} & D_{nd} \\ [0]_{2\times 3} & [I]_{2\times 2} \end{bmatrix},\ \tilde{B}_{nd} = \begin{bmatrix} B_{nd} \\ [0]_{2\times 2} \end{bmatrix} \tag{15}$$

where $[I]$ represents the identity matrix, and $[0]$ represents the zero matrix. W_k is the process noise vector of the disturbance accommodating system at step k.

4.2 Multi-rate output measurements

In the Kalman filter algorithm, output measurement is used for the correction stage. If lateral acceleration is selected as measurement, the output measurement equation is expressed as follows:

$$a_y = \frac{-\left(2C_f + 2C_r\right)}{M}\beta + \frac{\left(2l_r C_r - 2l_f C_f\right)}{Mu_x}\gamma \tag{16}$$

Due to the variation of tire cornering stiffness according to road condition (Fig. 2), lateral acceleration cannot provide accurate state estimation. In this paper, yaw rate and course angle are selected as output measurements. While the gyroscope can provide measurement every 1 millisecond, sampling time of course angle is much longer because of the limitation of the GPS receiver. For fair comparison with the methods in [12-14], 5 Hz update mode is set for the GPS receiver. This yields the course angle sampling of T_s = 200 milliseconds. The estimation steps between two consecutive updates of course angle are named "inter-samples". Based on the relation between course angle, yaw angle and sideslip angle, the output measurement equation is expressed as (17). The observation matrix is switched between two cases as in (18): if course angle is updated and during inter-samples.

$$Y_k = \tilde{C}_{nd} X_k + V_k = \begin{bmatrix} \gamma_{gyro,k} & v_{GPS,k} \end{bmatrix}^T \tag{17}$$

$$\begin{cases} \tilde{C}_{nd} = \begin{bmatrix} 0 & 1 & 0 & 0 & 0 \\ 1 & 0 & 1 & 0 & 0 \end{bmatrix} \text{ course angle update} \\ \tilde{C}_{nd} = \begin{bmatrix} 0 & 1 & 0 & 0 & 0 \\ 0 & 0 & 0 & 0 & 0 \end{bmatrix} \text{ during inter-samples} \end{cases} \tag{18}$$

In (17), V_k is the measurement noise vector at step k. Output measurement equation (17) does not rely on tire cornering stiffness. This is the advantage of using course angle in sideslip angle estimation. The observability of sideslip angle and disturbance terms are assured by checking the rank of matrix $\begin{bmatrix} \tilde{C}_{nd} & \tilde{C}_{nd}\tilde{A}_{nd} & \cdots & \tilde{C}_{nd}\tilde{A}_{nd}^4 \end{bmatrix}^T$. If the GPS signal is unavailable, accurate yaw angle estimation is impossible. Even though, sideslip angle and the disturbance terms can be estimated using only yaw rate sensor. Therefore, lateral stability control can be realized in case that GPS signal is lost.

4.3 Noise covariance matrices

Q_W and R_V are process noise and measurement noise covariance matrices, respectively. Q_W represents the accuracy of dynamical model and R_V shows the level of confidence placed in sensor measurements. In principle, the covariance matrices are not necessarily diagonal. In order to reduce the computational time when implementing the algorithm in the real-time control system, Q_W and R_V are treated as diagonal matrices as follows:

$$Q_W = \text{diag}\begin{bmatrix} Q_\beta, Q_\gamma, Q_\psi, Q_{d_1}, Q_{d_2} \end{bmatrix} \tag{19}$$

$$R_V = \text{diag}\begin{bmatrix} R_\gamma, R_v \end{bmatrix} \tag{20}$$

If R_V is set too large, the Kalman gain will decrease, thus, the estimation fails to update the propagated disturbances based on measurements. On the other hand, small Q_W results in unstable estimation, while large Q_W will force the estimation to completely rely upon the measurements, leading to measurement noise being directly transmitted into the estimated states. While R_γ is almost constant, R_v relies on the working condition of GPS receiver. According to GPS technology, the relative satellite-receiver geometry plays an important role in accuracy of positioning. R_v can be adjusted in real-time based on the dilution of precision of the GPS receiver. This problem will be addressed in future works. In this paper, trial-and-error method was conducted to select the suitable noise covariance matrices.

4.4 Kalman filter algorithm

The Kalman filter algorithm shown in Fig. 5 includes two stages:

1) Prediction based on the disturbance accommodating dynamic model.
2) Correction based on multi-rate measurements. Therefore, the algorithm is named disturbance accommodating multi-rate Kalman filter (DAMRKF) in this paper.

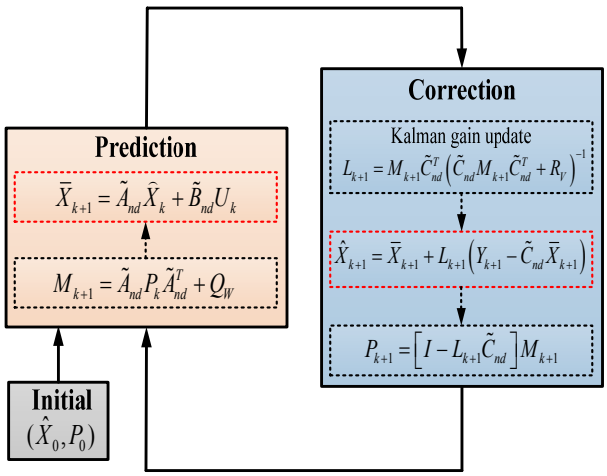

Fig. 5. Kalman filter algorithm

5. Lateral Stability Control Design

In this section, lateral stability control system of in-wheel motored electric vehicle is proposed. The general control system is shown in Fig. 6, and can be summarized as follows.

1) The reference model is obtained from the linear bicycle model.
2) The DAMRKF designed in the previous section provides the estimated values of sideslip angle, yaw rate and the disturbance terms that incorporate model error and external disturbances.
3) The purpose of the lateral stability control is to make the vehicle follow the desired trajectory. The system has two layers. In the upper layer, a new control

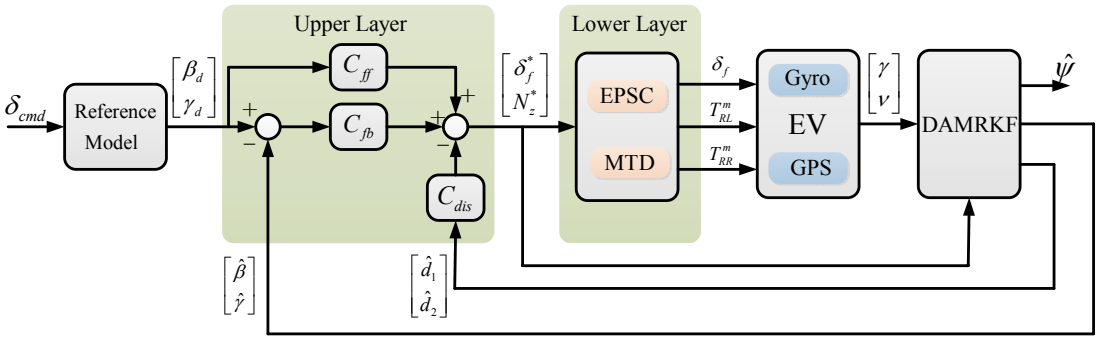

Fig. 6. Lateral stability control system based on disturbance accommodating multi-rate Kalman filter

scheme is proposed for yaw rate and sideslip angle tracking. In order to guarantee the robustness of the system, the upper layer is designed as a combination of 2-DOF control configuration and disturbance rejection. The upper layer outputs the yaw moment command and front steering angle commands to the lower layer including electric power steering control (EPSC) and the motor torque distribution (MTD).

5.1 Reference model

The reference model is determined based on the steady state response of sideslip angle and yaw rate from the front steering command given by the driver. From (1), (2), and using the nominal cornering stiffness, the desired values are calculated as follows:

$$\beta_d = \frac{1-\dfrac{M}{2\left(l_f+l_r\right)}\dfrac{l_f}{C_{rn}l_r}u_x^2}{1+Gu_x^2}\frac{l_r}{\left(l_f+l_r\right)}\delta_{cmd} \tag{21}$$

$$\gamma_d = \frac{1}{1+Gu_x^2}\frac{u_x}{\left(l_f+l_r\right)}\delta_{cmd} \tag{22}$$

$$G = \frac{M}{2\left(l_f+l_r\right)^2}\frac{C_{rn}l_r-C_{fn}l_f}{C_{fn}C_{rn}} \tag{23}$$

5.2 Upper control layer design

In [8], both yaw rate and sideslip angle are controlled only by yaw moment generated by the in-wheel motors. Therefore, there is a "trade-off" between sideslip angle control and yaw rate control. In [11, 16], and [17], active front steering is integrated with direct yaw moment control by different schemes. In [11], decoupling control method is utilized such that sideslip angle is controlled by front steering angle and yaw rate is controlled by yaw moment. It means the decoupling terms are designed in the upper control layer. As discussed in [16] and [17], the decoupling control is not robust enough under the variation of cornering stiffness. In case of big cornering stiffness error, i.e., 30% of the true value, the state responses will have a terrible oscillation about the desired values. Based on disturbance observer theory, in [16] and [17], a new decoupling control scheme is proposed with high robustness under model error. This scheme is a combination of yaw moment observer and lateral force observer that can compensate the lumped disturbances and nominalize the system as follows:

$$\begin{cases} \gamma = \dfrac{1}{I_{zn}}N_z \\ \beta = \dfrac{2C_{fn}}{M_n u_x s}\delta_f \end{cases} \tag{24}$$

Accurate sideslip angle is essential for lateral force observer. However, the problem of sideslip angle estimation was not solved in [16-17]. In this paper, we aim to propose a control scheme that can achieve two goals simultaneously: robust estimation of sideslip angle and robust lateral stability control. Thanks to the DAMRKF, sideslip angle and disturbance terms are estimated. While the estimated sideslip angle can be used for the 2-DOF control design, the estimated disturbance terms can be used to compensate the influence of model error. Moreover, it is unnecessary to decouple the two control inputs. Considering the controlled states as a vector of two components, model following control can be applied for obtaining the input vector.

Design of disturbance rejection

The dynamics of the lateral motion can be expressed as follows:

$$\begin{bmatrix}\dot{\beta}\\ \dot{\gamma}\end{bmatrix} = \begin{bmatrix}a_{n11} & a_{n12}\\ a_{n21} & a_{n22}\end{bmatrix}\begin{bmatrix}\beta\\ \gamma\end{bmatrix} + \begin{bmatrix}b_{n11} & b_{n12}\\ b_{n21} & b_{n22}\end{bmatrix}\begin{bmatrix}\delta_f\\ N_z\end{bmatrix} + \begin{bmatrix}d_1\\ d_2\end{bmatrix} \tag{25}$$

To compensate for the influence of the disturbances, the disturbance rejection matrix is designed as follows:

$$C_{dis} = \begin{bmatrix}b_{n11} & b_{n12}\\ b_{n21} & b_{n22}\end{bmatrix}^{-1} \tag{26}$$

With the disturbance rejection, the vehicle system's behavior is augmented to be the nominal model. Therefore, the robustness of the control system is improved. The feed-back and feed-forward controller are designed based on the nominal model for the tracking purpose.

Design of feed-forward controller

From (25), the transfer function from the control input vector to the controlled state vector is derived as follows:

$$P_n = \left(s[I]_{2\times 2} - \begin{bmatrix} a_{n11} & a_{n12} \\ a_{n21} & a_{n22} \end{bmatrix} \right)^{-1} \begin{bmatrix} b_{n11} & b_{n12} \\ b_{n21} & b_{n22} \end{bmatrix} \quad (27)$$

The detailed formulation of P_n is presented in the Appendix. The feed forward controller is designed as the inverse of P_n given by:

$$C_{ff} = P_n^{-1} = \begin{bmatrix} C_{ff11} & C_{ff12} \\ C_{ff21} & C_{ff22} \end{bmatrix} \quad (28)$$

Design of feed-back controller

The desired closed loop system including the feed-back controller and the plant is expressed as follows:

$$K = \begin{bmatrix} \dfrac{K_\beta}{s+K_\beta} & 0 \\ 0 & \dfrac{K_\gamma}{s+K_\gamma} \end{bmatrix} \quad (29)$$

In (29), the cut-off frequency K_β and K_γ were determined by trial-and-error experiments. If the cut-off frequencies are set too low, the responses of sideslip angle and yaw rate are too slow to track the desired values. On the other hand, it is impossible to set the cut-off frequencies too high, due to the limitation of the actuators.

$$\begin{aligned} &\left(I + P_n C_{fb}\right)^{-1} P_n C_{fb} = K \\ &\Rightarrow C_{fb} = P_n^{-1} K \left(I - K\right)^{-1} = \begin{bmatrix} C_{fb11} & C_{fb12} \\ C_{fb21} & C_{fb22} \end{bmatrix} \end{aligned} \quad (30)$$

The feedback controller augments the closed loop system to the desired model K with the poles placed at $-K_\beta$ and $-K_\gamma$. The internal stability of the system is assured by verifying the poles of the following matrices of transfer function:

$$P_n^{-1}\left(I + P_n C_{fb}\right)^{-1} P_n C_{fb} \text{ and } \left(P_n C_{fb}\right)^{-1}\left(I + P_n C_{fb}\right)^{-1} P_n C_{fb}$$

Finally, the control commands are obtained as follows:

$$\begin{bmatrix} \delta_f^* \\ N_z^* \end{bmatrix} = C_{fb} \begin{bmatrix} \beta_d - \hat{\beta} \\ \gamma_d - \hat{\gamma} \end{bmatrix} + C_{ff} \begin{bmatrix} \beta_d \\ \gamma_d \end{bmatrix} - C_{dis} \begin{bmatrix} \hat{d}_1 \\ \hat{d}_2 \end{bmatrix} \quad (31)$$

5.3 Lower control layer design

Yaw moment is generated by the difference between the rear-left and rear-right in-wheel motors. The torque commands are distributed to two rear in-wheel motors by solving the following equations in real time:

$$\begin{cases} \dfrac{d_r}{2}\left(\dfrac{T_{RR}^m}{r} - \dfrac{T_{RL}^m}{r}\right) = N_z^* \\ T_{RR}^m + T_{RL}^m = T_{cmd} \end{cases} \quad (32)$$

where r is the wheel radius, T_{cmd} is the torque command given by the driver, and d_r is the track-width between two rear wheels. T_{RL}^m and T_{RR}^m are the rear-left and rear-right in-wheel motor's torque, respectively.

An EPS motor is utilized for generating the front steering angle (Fig. 7). This system enables the steer-by-wire mode for manipulating the vehicle without the driver's handling.

Fig. 7. Front EPS motor system

6. Simulation Results

Based on the vehicle specification in Table II, vehicle model was constructed using Matlab/Simulink. The sampling time of simulation is set to 1 millisecond to match that of the experiment condition.

6.1 Sideslip angle estimation results

In this simulation, we verify the proposed Kalman filter in comparison with other estimation methods. Two cases of driving are simulated: cornering test and lane-change test with sinusoidal steer command. In both cases, the following driving conditions were set:

1) The longitudinal velocity is 25 km/h.
2) From 4 second, a strong lateral wind force starts to act on the vehicle. It introduces lateral force disturbance F_d

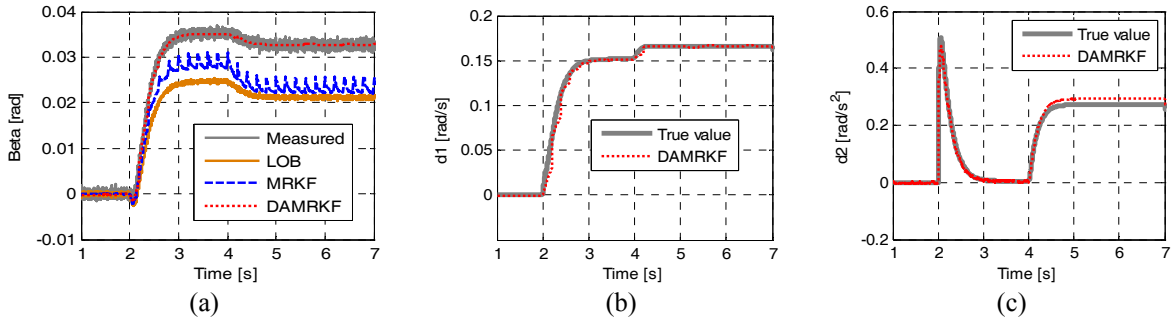

(a) (b) (c)

Fig. 8. Simulation results of sideslip angle estimation: *Cornering test*.
(a) Sideslip angle; (b). Disturbance term d_1; (c). Disturbance term d_2.

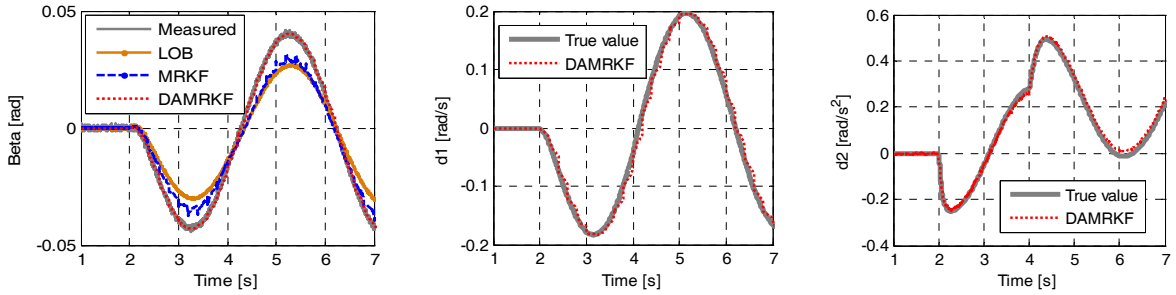

(a) (b) (c)

Fig. 9. Simulation results of sideslip angle estimation: *Lane-change test*.
(a) Sideslip angle; (b). Disturbance term d_1; (c). Disturbance term d_2.

and yaw moment disturbance N_d.

3) The cornering stiffness of vehicle model are $C_f = C_r =$ 7000 N/rad. However, the estimation model is designed with the nominal values $C_{fn} = C_{rn}$=10,000 N/rad. This means a big error is introduced to cornering stiffness of the estimation model.
4) The disturbance terms d_1 and d_2 are simulated using (8) and (9).
5) The DAMRKF is compared to the following two methods. The first is the sideslip angle estimation using linear observer (LOB) with constant cornering stiffness model, as described in [8]. Yaw rate and lateral acceleration are selected as output measurements. The second method is multi-rate Kalman filter (MRKF) proposed in [13]. This method uses the yaw rate and course angle as output measurement.

Simulation results of two tests, cornering test and lane change test, are shown in Fig. 8 and Fig. 9, respectively. The results include sideslip angle estimations and disturbance estimations. The influence of lateral wind force can be demonstrated by the change of sideslip angle and disturbance terms from 4 second. In both tests, LOB shows the poorest estimation performance. By using course angle from GPS, MRKF provides better estimation than LOB. However, the results degrade under the influence of both model error and lateral wind force. By using the proposed DAMRKF method, the disturbances are estimated as the extended states. Although the tracking of disturbance estimation is not perfect, sideslip angle estimation performance is improved considerably. Therefore, the assumption of the dynamics of disturbances in (12) is acceptable.

6.2 Lateral Stability Control Results

After evaluating the estimation algorithm, the Matlab/Simulink model of the whole system in Fig. 6 is constructed. Fig. 10 demonstrates vehicle motion with step steer command. The simulation conditions were set the same as the previous sub-section (under model error and lateral wind force). In the case of without lateral stability control, vehicle motion is handled by only driver's steer command. In this case, both the yaw rate and the side slip angle increases considerably in comparison with the desired values. In contrast, with the proposed control system, active front steering and yaw moment are generated to control the sideslip angle and the yaw rate to follow their desired values.

7. Experimental Results

7.1 Sideslip angle estimation results

Before implementing the control algorithm, experiments were conducted with driver's command input only. Based on the experimental results, trial-and-error method was

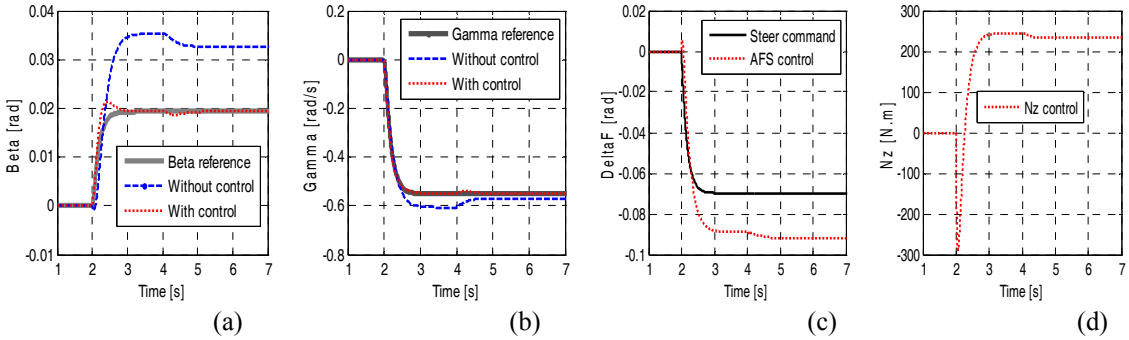

Fig. 10. Simulation results of lateral stability control based on DAMRKF: *Cornering test*.
(a) Sideslip angle; (b). Yaw rate (c); Front steering angle; (d). Yaw moment.

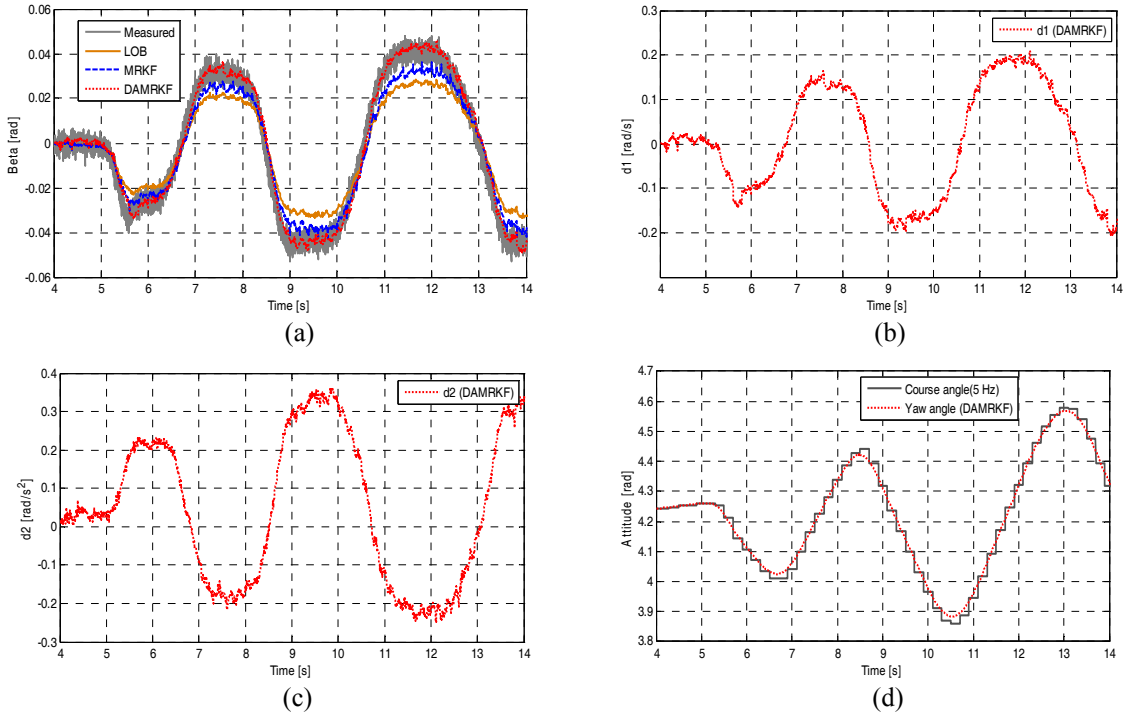

Fig. 11. Experiment results of sideslip angle estimation: *Lane-change test*.
(a) Sideslip angle; (b) Disturbance term d_1; (c) Disturbance term d_2; (d) Course angle.

used to select the suitable noise covariance matrices for Kalman filter design. Like the simulation, the nominal cornering stiffness of the estimation model is set as C_{fn} = C_{rn} = 10,000 N/rad. The cornering stiffness according to road condition is approximately $C_f = C_r \approx 7000$ N/rad. The velocity of vehicle on this test is controlled at about 20 km/h. During the test, wind force introduced the unknown input disturbances to the estimation system. Sideslip angle estimation results are shown in Fig. 11 (a). As the simulation, LOB has largest estimation error in comparison with the sideslip angle obtained from optical sensor. MRKF is shown to be superior, but it is still sensitive to model errors and disturbances. The proposed DAMRKF, on the other hand, is robust to both model errors and disturbances. The disturbance terms estimated by this method are shown in Figs. 11 (b-c). Fig. 11 (d) shows the course angle measured by GPS receiver and the estimated yaw angle by DAMRKF. While yaw angle was estimated every 1 millisecond, the sampling time of course angle from GPS was 200 milliseconds. This is another advantage of the proposed DAMRKF.

7.2 Lateral stability control results

In this sub-section, results of cornering test are shown. Instead of handling by the driver, steer-by-wire mode is used for generating front steering angle. The steering command is pre-designed and generated by the program.

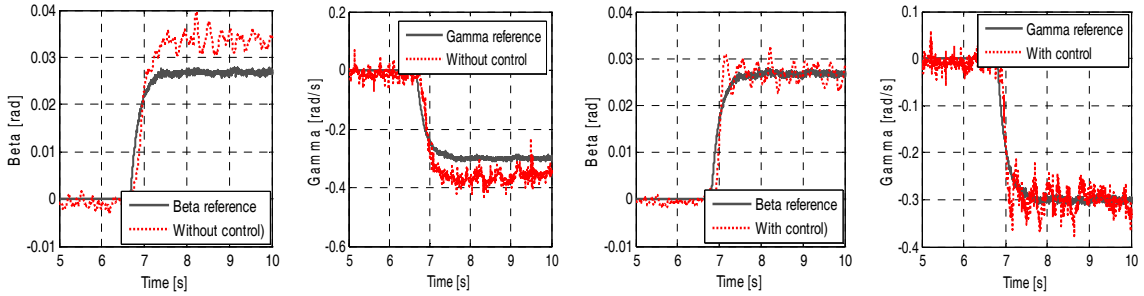

(a) (b) (c) (d)

Fig. 12. Experiment results of lateral stability control based on DAMRKF: *Cornering test*.: (a) Sideslip angle (*without control*); (b) Yaw rate (*without control*); (c) Sideslip angle (*with control*); (d) Yaw rate (*with control*).

The velocity of vehicle in this experiment is 18 km/h. By this way, the same driving condition is made for the cases of with stability control and without stability control. Fig. 12 shows that, in case of without control, both sideslip angle and yaw rate increases over the desired values. When the proposed control system was applied, sideslip angle and yaw rate follows the reference model. This means that the stability of the EV is improved.

8. Conclusions

The most important contribution of this paper is a new method for robust estimation of sideslip angle using a single antenna GPS receiver and yaw rate sensor. By applying the disturbance accommodating idea, accurate estimation was achieved even under model error and external disturbance. The effectiveness of the proposed DAMRKF was demonstrated by both simulations and experiments. Moreover, DAMRKF was successfully implemented in a lateral stability control system of electric vehicle with rear in-wheel motors and front active steering. Based on the DAMRKF, a new scheme for combining front steering and yaw moment control was proposed. It is a combination of 2-DOF control and disturbance rejection. DAMRKF kills two birds with one stone by providing not only accurate state estimates but also disturbance estimates for improving control robustness. However, the following questions still remain: 1) How to improve the multi-rate estimation because during inter-samples there are no new updates of measurement based on GPS. 2) How to tune the noise covariance according to GPS measurement in real time. These problems will be solved in future works to fulfill the algorithm of vehicle state estimation using GPS.

Acknowledgements

The authors would like to thank Japan Radio Co. Ltd. for supporting GPS receiver CCA-600.

Appendix: Lateral Dynamic Derivation

The components of the matrices that represent lateral dynamic motion are calculated as follows:

$$\begin{bmatrix} a_{n11} & a_{n12} \\ a_{n21} & a_{n22} \end{bmatrix} = \begin{bmatrix} \dfrac{-2\left(C_{fn}+C_{rn}\right)}{Mu_x} & -1-\dfrac{2\left(C_{fn}l_f-C_{rn}l_r\right)}{Mu_x^2} \\ \dfrac{-2\left(C_{fn}l_f-C_{rn}l_r\right)}{I_z} & \dfrac{-2\left(C_{fn}l_f^2+C_{rn}l_r^2\right)}{I_z u_x} \end{bmatrix} \tag{33}$$

$$\begin{bmatrix} b_{n11} & b_{n12} \\ b_{n21} & b_{n22} \end{bmatrix} = \begin{bmatrix} \dfrac{2C_{fn}}{Mu_x} & 0 \\ \dfrac{2C_{fn}l_f}{I_z} & \dfrac{1}{I_z} \end{bmatrix} \tag{34}$$

The nominal model is derived as follows:

$$\begin{cases} P_{n11} = \dfrac{b_{n11}s+b_{n21}a_{n12}-b_{n11}a_{n22}}{(s-a_{n11})(s-a_{n22})-a_{n12}a_{n21}} \\ P_{n12} = \dfrac{b_{n22}a_{n12}}{(s-a_{n11})(s-a_{n22})-a_{n12}a_{n21}} \\ P_{n21} = \dfrac{b_{n21}s+b_{n11}a_{n21}-b_{n21}a_{n11}}{(s-a_{n11})(s-a_{n22})-a_{n12}a_{n21}} \\ P_{n22} = \dfrac{b_{n22}s-b_{n22}a_{n11}}{(s-a_{n11})(s-a_{n22})-a_{n12}a_{n21}} \end{cases} \tag{35}$$

The components of the feed-forward and feed-back controllers are expressed as follows:

$$\begin{cases} C_{ff11} = \dfrac{\left(b_{n22}s-b_{n22}a_{n11}\right)}{b_{n11}b_{n22}} \\ C_{ff12} = \dfrac{-a_{n12}}{b_{n11}} \\ C_{ff21} = \dfrac{\left(-b_{n21}s-b_{n11}a_{n21}+b_{n21}a_{n11}\right)}{b_{n11}b_{n22}} \\ C_{ff22} = \dfrac{\left(b_{n11}s+b_{n21}a_{n12}-b_{n11}a_{n22}\right)}{b_{n11}b_{n22}} \end{cases} \tag{36}$$

$$\begin{cases} C_{fb11} = \dfrac{\left(b_{n22}s - b_{n22}a_{n11}\right)\left(s+K_\gamma\right)}{b_{n11}b_{n22}s}\dfrac{K_\beta}{s+K_\beta} \\ C_{fb12} = \dfrac{-a_{n12}\left(s+K_\beta\right)}{b_{n11}s}\dfrac{K_\gamma}{s+K_\gamma} \\ C_{fb21} = \dfrac{\left(-b_{n21}s - b_{n11}a_{n21} + b_{n21}a_{n11}\right)\left(s+K_\gamma\right)}{b_{n11}b_{n22}s}\dfrac{K_\beta}{s+K_\beta} \\ C_{fb22} = \dfrac{\left(b_{n11}s + b_{n21}a_{n12} - b_{n11}a_{n22}\right)\left(s+K_\beta\right)}{b_{n11}b_{n22}s}\dfrac{K_\gamma}{s+K_\gamma} \end{cases} \quad (37)$$

References

[1] Y. Hori, "Future Vehicle Driven By Electricity and Control-Research on 4 Wheel Motored UOT March II," *IEEE Transactions on Industrial Electronics*, Vol. 51, No. 5, pp. 954-962, 2004.

[2] R. Rajamani, Vehicle Dynamics and Control, New York: Springer-Verlag, 2005.

[3] B. C. Chen, F.C. Hsieh, "Sideslip Angle Estimation Using Extended Kalman Filter," *Vehicle System Dynamics*, Vol. 46, No. 1, pp. 353-364, 2008.

[4] D. N. Piyabongkarn, R. Rajamani, J. A. Grogg, and Jae Y. Lew, "Development and Experimental Evaluation of Slip Angle Estimator for Vehicle Stability Control," *IEEE Transactions on Control Systems Technology*, Vol. 17, No. 3, pp. 78-88, 2009.

[5] L. Imsland, T. A. Johansen, T. I. Fossen, H. F. Grip, J. C. Kalkkuhl, and A. Suissa, "Vehicle Velocity Estimation Using Nonlinear Observers," *Auto-matica*, Vo. 42, Issue 12, pp. 2091-2103, 2006.

[6] J. Stephant, A. Charara, and D. Meizei, "Evaluation of a Sliding Model Observer for Vehicle Sideslip Angle," *Control Engineering Practice*, Vol. 15, No. 7, pp. 803-812, 2007.

[7] U. Kiencke and A. DaiB, "Observation of Lateral Vehicle Dynamics," *Control Engineering Practice*, Vol. 5, No. 8, pp. 1145-1150, 1997.

[8] C. Geng, L. Mostefai, M. Denai, and Y. Hori, "Direct Yaw Moment Control of an In Wheel Motored Electric Vehicle Based on Body Slip Angle Fuzzy Observer," *IEEE Transactions on Industrial Electronics*, Vol. 56, No. 5, pp. 1411-1419, 2009.

[9] F. Cheli, E. Sabbioni, M. Pesce, and S. Melzi, "A Methodology for Vehicle Slip Angle Identification: Comparison with Experimental Data," *Vehicle System Dynamics*, Vol. 45, No. 6, pp. 549-563, 2010.

[10] Y. Wang, B. M. Nguyen, P. Kotchapansompote, H. Fujimoto, and Y. Hori, "Image-Processing-Based State Estimation for Lateral Control of Electric Vehicle Using Multi-Rate Kalman Filter," *Recent Patents on Signal Processing*, Vol. 2, No. 2, pp. 140-148, 2012.S.

[11] K. Nam, H. Fujimoto, and Y. Hori, "Lateral Stability Control of In-Wheel-Motor-Driven Electric Vehicles Based on Sideslip Angle Estimation Using Lateral Tire Force Sensors," IEEE Transactions on Vehicular Technology, Vol. 61, No. 5, pp. 1972-1985, 2012.

[12] D. M. Bevly, J. Ryu, and J. C. Gerdes, "Integrating INS Sensors With GPS Measurements for Continuous Estimation of Vehicle Sideslip, Roll, and Tire Cornering Stiffness," *IEEE Transactions on Intelligent Transportation System*, Vol. 7, No. 4, pp. 483-493, 2006.

[13] R. Anderson and D. M. Bevly, "Using GPS with a Model-Based Estimator to Estimate Critical Vehicle States," *Vehicle System Dynamics*, Vo. 48, No. 12, pp. 1413-1438, 2010.

[14] J. H. Yoon and H. Peng, "Sideslip Angle Estimation Based on GPS and Magnetometer Measurements," *Proceeding of 11th International Symposium on Advanced Vehicle Control* (AVEC), Korea, 2012.

[15] C. Johnson, "Accommodation of External Disturbances in Linear Regulator and Servomechanism Problem," *IEEE Transaction on Automatic Control*, Vol. 16, No. 6, pp. 535-644, 1971.

[16] Y. Yamauchi and H. Fujimoto, "Vehicle Motion Control Method Using Yaw Moment Observer and Lateral Force Observer for Electric Vehicle," IEEJ Transactions on Industry Applications, Vol. 130, No. 8, pp. 939-944, 2010.

[17] H. Fujimoto and Y. Yamauchi, "Advanced Motion Control of Electric Vehicle Based on Lateral Force Observer with Active Steering," *Proceeding of 2010 IEEE International Symposium on Industrial Electronics* (ISIE), pp. 3627-3632, 2010.

Binh Minh Nguyen was born in Haiphong, Vietnam. He is currently working toward the Ph.D. degree in the Department of Advanced Energy, Graduate School of Frontier Sciences, the University of Tokyo. His current research interests include robust control theory, sensor fusion, motion control of electric vehicle, visual servo system.

Yafei Wang received the Ph.D. degree in Electrical Engineering from the University of Tokyo, Tokyo, Japan, in 2013. From 2008 to 2010, he worked in automotive industry for nearly 2 years, including internships with Caterpillar Remanufacturing Services (Shanghai) and FIAT Powertrain Technologies (Shanghai), and full-time experience with Delphi China Technical Center (Shanghai). Currently, he is working as a postdoctoral researcher in the University of Tokyo. He is interested in state estimation and motion control for electric vehicles, multi-rate estimation theory, and real-time image processing.

Hiroshi Fujimoto received the Ph.D. degree from The University of Tokyo, Tokyo, Japan, in 2001. In 2001, he joined the Department of Electrical Engineering, Nagaoka University of Technology, Niigata, Japan, as a Research Associate. From 2002 to 2003, he was a Visiting Scholar with the School of Mechanical Engineering, Purdue University, West Lafayette, IN. In 2004, he joined the Department of Electrical and Computer Engineering, Yokohama National University, Yokohama, Japan, as a Lecturer, and he became an Associate Professor in 2005. He has been an Associate Professor with the Department of Advanced Energy, Graduate School of Frontier Sciences, The University of Tokyo, since 2010. His research interests include control engineering, motion control, nanoscale servo systems, electric vehicle control, and motor drives.

Dr. Fujimoto is a Member of the Institute of Electrical Engineers of Japan, the Society of Instrument and Control Engineers (SICE), the Robotics Society of Japan, and the Society of Automotive Engineers of Japan. He received the Best Paper Award from the IEEE TRANSACTION ON INDUSTRIAL ELECTRONICS in 2001, the Isao Takahashi Power Electronics Award in 2010, and the Best Author Prize from the SICE in 2010.

Yoichi Hori received the B.S., M.S., and Ph.D. degrees in electrical engineering from The University of Tokyo, Tokyo, Japan, in 1978, 1980, and 1983, respectively. In 1983, he joined the Department of Electrical Engineering, the University of Tokyo, as a Research Associate, where he later became an Assistant Professor, an Associate Professor, and, in 2000, a Professor. He moved to the Institute of Industrial Science as a Professor with the Information and System Division in 2002 and to the Department of Advanced Energy, Graduate School of Frontier Sciences, The University of Tokyo, in 2008. From 1991 to 1992, he was a Visiting Researcher with the University of California, Berkeley. His research interests are control theory and its industrial applications to motion control, mechatronics, robotics, electric vehicles, etc.

Dr. Hori has been the Treasurer of the IEEE Japan Council and Tokyo Section since 2001. He is also an Administrative Committee member of the IEEE Industrial Electronics Society and a member of the Society of Instrument and Control Engineers, the Robotics Society of Japan, the Japan Society of Mechanical Engineers, and the Society of Automotive Engineers of Japan (JSAE). He was the President of the Industry Applications Society of the Institute of Electrical Engineers of Japan (IEEJ), the President of Capacitors Forum, the Chairman of the Motor Technology Symposium of the Japan Management Association, and the Director on Technological Development of JSAE. He received the Best Transactions Paper Award from the IEEE TRANSACTION ON INDUSTRIAL ELECTRONICS in 1993 and 2001, the 2000 Best Transactions Paper Award from the IEEJ, and the 2011 Achievement Award from the IEEJ.